Erciyes University Journal of Institue Of Science and Technology

Highly Selective and Polarization-Independent Band-Pass FSS with Robust Angular Stability for Secure CubeSat Communications

Research Article
10.65520/erciyesfen.1919953

Imprint:
Volume: 42(2)
Year: 2026
Page: 685-700

Mustafa GÜÇ[a]
Mert KARAHAN[b*]
Habib JAMALOV[c]
Galip Orkun ARICAN[d]

[a] Master's Student, National Defence University, guc.mustafa4188@gmail.com
[b] Asst. Prof., National Defence University, mertkarahan@outlook.com
[c] Master's Student, National Defence University, habibjamalov@gmail.com
[d] PhD., ASELSAN Inc, goarican@aselsan.com

[*] Corresponding Author

Received: 3/31/2026
Accepted: 7/3/2026

Citation:
Mustafa GÜÇ, Mert KARAHAN, Habib JAMALOV, Galip Orkun ARICAN (2026). Highly Selective and Polarization-Independent Band-Pass FSS with Robust Angular Stability for Secure CubeSat Communications. *Erciyes University Journal of Institute Of Science and Technology*, 42(2), 685-700. https://doi.org/10.65520/erciyesfen.1919953

Abstract

This paper presents the design, fabrication, and experimental validation of a highly selective, polarization-independent band-pass Frequency Selective Surface (FSS) tailored for secure CubeSat communications. As the electromagnetic (EM) spectrum becomes increasingly congested, mitigating unintentional interference and intentional jamming in space-based systems is critical. The proposed FSS unit cell, featuring a compact footprint of 10 x 10 mm^2, is developed through a hybrid geometric approach combining a square loop with straight and cross-dipoles. At normal incidence, it exhibits a high-selectivity pass-band in the 6.2–9.1 GHz range with a fractional bandwidth of 40.03% and a maximum roll-off rate of 40.15 dB/GHz, supporting selective transmission within the targeted satellite communication band. Simultaneously, it provides dual band-stop responses at 4–4.7 GHz and 15–17.3 GHz, with a peak shielding effectiveness exceeding 45 dB for out-of-band EM suppression. Full-wave TE/TM simulations indicate that the structure maintains a stable center-resonance behavior for oblique incidence angles up to 60°, while the four-fold rotational symmetry contributes to polarization-insensitive operation with cross-polarization levels below -20 dB. To verify the design, a physical prototype was manufactured and characterized using a free-space measurement setup within a controlled clean-room environment. The agreement between the simulated and measured normal-incidence responses supports the potential of the proposed FSS as a compact EM filtering and shielding candidate for CubeSat-oriented communication systems.

Keywords: *Frequency selective surface (FSS), band-pass filter, secure satellite communication, angular stability, polarization-independent, CubeSat*

Güvenli Küp Uydu Haberleşmesi İçin Yüksek Seçicilikli, Polarizasyondan Bağımsız ve Açısal Kararlı Bant Geçiren FSY Tasarımı

Öz

Bu çalışma, güvenli Küp Uydu haberleşmeleri için uyarlanmış yüksek seçiciliğe sahip, polarizasyondan bağımsız bant geçiren bir Frekans Seçici Yüzey'in (FSY) tasarımını, üretimini ve deneysel doğrulamasını sunmaktadır. Elektromanyetik (EM) spektrumun giderek yoğunlaşmasıyla birlikte, uzay tabanlı sistemlerde kasıtsız girişimin ve kasıtlı karıştırmanın azaltılması kritik bir gereklilik haline gelmiştir. 10 x 10 mm^2'lik kompakt bir boyuta sahip olan önerilen FSY birim hücresi, kare halka ile düz ve çapraz dipolleri birleştiren hibrit bir geometrik yaklaşımla geliştirilmiştir. Normal geliş açısında yapı, 6.2–9.1 GHz aralığında %40.03 kesirli bant genişliğine ve 40.15 dB/GHz maksimum kesim eğimine

Screened by iThenticate for Authors & Researchers

sahip yüksek seçicilikte bir geçirme bandı sergileyerek hedeflenen uydu haberleşme bandında seçici iletimi desteklemektedir. Bununla birlikte, yapı 4–4.7 GHz ve 15–17.3 GHz aralıklarında çift bant-durdurma yanıtı sağlamakta ve bant dışı EM bastırma için 45 dB'nin üzerinde tepe ekranlama etkinliği sunmaktadır. Tam dalga TE/TM simülasyonları, yapının 60°'ye kadar eğik geliş açılarında merkez rezonans davranışını kararlı biçimde koruduğunu göstermekte; dört katlı rotasyonel simetri ise -20 dB'nin altında çapraz polarizasyon seviyeleriyle polarizasyondan bağımsız çalışmaya katkı sağlamaktadır. Tasarımı doğrulamak amacıyla fiziksel bir prototip üretilmiş ve kontrollü temiz oda ortamında serbest uzay ölçüm düzeneği kullanılarak karakterize edilmiştir. Simülasyon sonuçları ile normal geliş açısında elde edilen ölçüm sonuçları arasındaki uyum, önerilen FSY'nin Küp Uydu odaklı haberleşme sistemleri için kompakt bir EM filtreleme ve ekranlama adayı olarak potansiyelini desteklemektedir.

Anahtar kelimeler: *Frekans seçici yüzey (FSY), bant geçiren filtre, güvenli uydu haberleşmesi, açısal kararlılık, polarizasyondan bağımsız, Küp Uydu (KüpSat)*

1. INTRODUCTION

Parallel to the rapid advancements in technology, the proliferation of electronic systems has intensified the utilization and complexity of the Electromagnetic (EM) Spectrum. These systems, which hold critical importance in both civilian and military domains, constitute the backbone of advanced communication networks, radar technologies, and the rapidly expanding field of satellite systems. The dense and simultaneous occupancy of the spectrum leads to undesired EM interference (EMI) between diverse frequency bands, thereby reducing communication channel capacities and compromising operational reliability [1]. In this context, the development of Frequency Selective Surfaces (FSS) capable of isolating target frequency bands with high efficiency while maintaining signal integrity has become a necessity for ensuring robust and sustainable EM compatibility (EMC).

To minimize the mutual interference between various communication environments and to extend coverage to a global scale, communication infrastructures have inevitably shifted toward space-based systems. At the core of this evolution, satellite communication has transitioned from a supplementary element to the primary medium for both civilian and military operations. Particularly in the military domain, all network-centric structures, including fire support systems, have become heavily dependent on high-speed satellite links [2]. This paradigm shift in defense strategies has led emerging nations, alongside developed ones, to increase their presence in the space environment. Consequently, space has evolved from being solely a domain for scientific discovery into a strategic and military arena of competition. However, the geometric increase in the number of satellites and spectral density introduces significant risks of noise, EMI, and intentional electronic jamming, thereby threatening the sustainability and security of space-based communications.

Providing uninterrupted and high-quality service in both military and civilian applications remains a challenging requirement for end-users. Considering the density of the EM spectrum, reducing both intentional and unintentional interference that degrades system performance is a key design requirement. In light of advancing design and manufacturing techniques, FSS have emerged in recent years as effective tools for addressing these complex EM challenges [3], [4]. Current research in FSS technology specifically focuses on achieving stable frequency responses regardless of the signal incidence angle (angular stability), the reduction of unit cell dimensions (miniaturization), and the capability to operate across multiple resonance frequencies [5], [6], [7]. Comprehensive reviews in the literature further emphasize the relevance of such advanced FSS designs for next-generation telecommunication and shielding applications [8].

Despite these recent advancements, existing FSS designs frequently encounter significant performance trade-offs. For instance, while some structures in the literature achieve extreme miniaturization or wideband operation, they often compromise on frequency selectivity, exhibiting poor roll-off rates that are inadequate for densely packed spectra [9], [10]. Similarly, designs focusing primarily on angular stability sometimes struggle to provide deep out-of-band shielding effectiveness, or they lack explicitly validated cross-polarization isolation at high oblique incidences up to 60° [11], [12]. Addressing these literature gaps requires a balanced approach that can simultaneously deliver sharp frequency selectivity, a compact footprint, and robust polarization insensitivity without structural complexity.

In this study, a novel FSS structure is designed and experimentally validated for secure CubeSat communication systems operating in space environments, providing high-selectivity transmission in the targeted communication band while exhibiting dual stop-band characteristics. Within the 0–18 GHz spectrum, the FSS is engineered to provide a high-selectivity pass-band in the 6.2–9.1 GHz range—encompassing the targeted 7–9 GHz secure satellite links—and deep band-stop responses at other frequencies to mitigate interference [13], [14]. The 10 x 10 mm^2 unit cell geometry was achieved through a hybrid combination of square loop and cross-dipole elements, incorporating a four-fold rotational symmetry for inherent polarization independence. A key advantage of the proposed structure is its ability to maintain stable core filtering performance up to 60° for both transverse electric (TE) and transverse magnetic (TM) modes [15], [16]. The organization of the paper is as follows: Section II discusses the geometric evolution and parametric studies; Section III presents the analysis of simulation results; Section IV details the fabrication process and experimental measurement results; and the final section provides a comprehensive evaluation of the findings.

2. DESIGN AND ANALYSIS OF THE FSS STRUCTURE

The geometrical configuration of the proposed FSS unit cell is systematically developed through a hybrid structural approach. The top and side views of the finalized structure are illustrated in Fig. 1, whereas the step-by-step evolutionary stages of the design are depicted as insets (a) through (d) within the reflection coefficient (S_{11}) graph in Fig. 2. Initially (Fig. 2, inset a), a central square loop with an internal slot was designed, accompanied by a plus-shaped cross-dipole positioned within the aperture. In the subsequent step (Fig. 2, inset b), bent arms were extended from the corners of the square loop, and truncated patches were placed beneath these arms to manipulate the effective electrical length. Afterwards (Fig. 2, inset c), straight dipoles were integrated at the terminals of the bent arms and truncated patches to finely tune the resonance characteristics. Ultimately (Fig. 2, inset d), this base structure was duplicated using a 90° rotational symmetry around the origin, forming a complete four-fold symmetric unit cell. This four-fold symmetric architecture is a major factor contributing to the polarization-insensitive response and angular stability observed for both TE and TM incident waves.

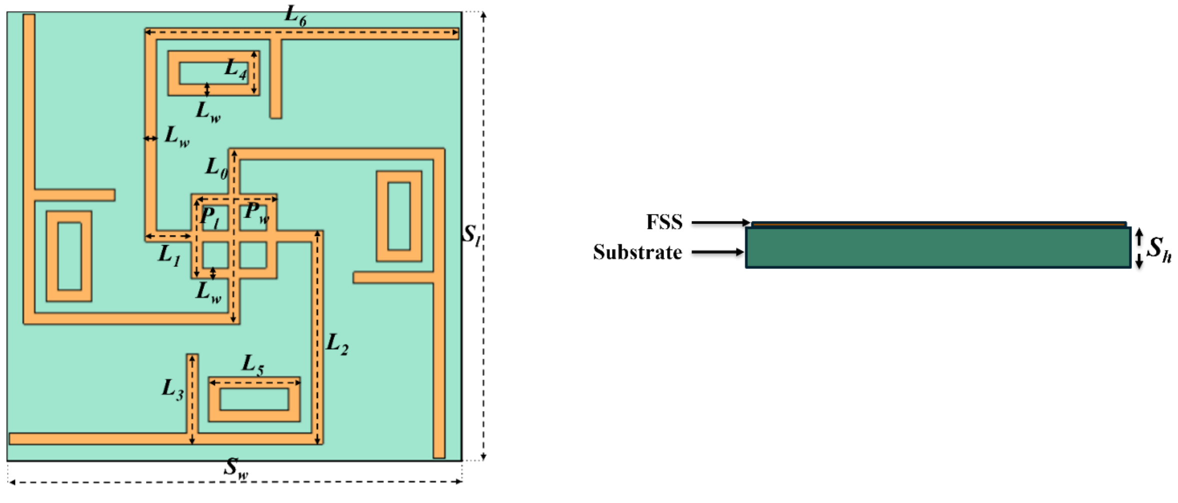

(a) (b)

Figure 1. *The proposed FSS unit cell geometry: (a) top view, (b) side view.*

The overall physical footprint of the proposed FSS unit cell is highly compact, with the outer dimensions measuring 10 *x* 10 mm^2 (S_w *x* S_l). As depicted in the top and side views in Fig. 1, the conductive patterns, including the square loop and bent arm structures, are modeled using copper with a thickness (C_h) of 0.035 mm. These metallic layers are etched on a low-loss Rogers RT5880 dielectric substrate, which is characterized by a relative permittivity (ε_r) of 2.2, a loss tangent (tanδ) of 0.0009, and a thickness (S_h) of 0.787 mm. The optimized geometrical parameters governing the unit cell are comprehensively listed in Table 1. Furthermore, Fig. 2 illustrates S_{11} characteristics corresponding to the sequential design stages, providing a comparative analysis of the structure's evolution.

Table 1. *Optimized design parameters of the proposed FSS unit cell.*

Parameter	Value (mm)	Parameter	Value (mm)
S_w	10	L_0	3.9
S_l	10	L_1	1.0
S_h	0.787	L_2	4.75
C_h	0.035	L_3	2.0
P_w	1.9	L_4	1.0
P_l	1.9	L_5	2.0
L_w	0.25	L_6	6.9

3. SIMULATION RESULTS

The full-wave EM simulations of the proposed FSS structure were performed using CST Studio Suite software. In this section, the frequency response, surface current distributions, parametric optimization, angular stability, and cross-polarization characteristics of the design are presented and discussed in detail.

3.1. Design Stage Analysis

Upon examining the reflection coefficient (S_{11}) characteristics presented in Fig. 2, the primary objectives behind each geometrical evolution can be clearly understood. Initially (Fig. 2a), the simple square loop structure exhibits a broad and shallow band-stop profile, acting primarily as a basic inductive element. The fundamental objective of integrating the bent arms (Fig. 2b) is to significantly elongate the effective electrical length of the surface currents, which increases the equivalent series inductance and shifts the primary resonance toward the lower frequency spectrum. Subsequently, the addition of the truncated patches (Fig. 2c) introduces strong capacitive coupling between adjacent unit cells. The objective of this added capacitance is to sharpen the transition bands, thereby causing the structure to evolve toward a more selective behavior. In the final stage, the incorporation of straight dipoles (Fig. 2d) is aimed at fine-tuning the equivalent LC circuit. These dipoles adjust the mutual coupling and help place the high-selectivity band-pass response within the targeted 7–9 GHz X-band.

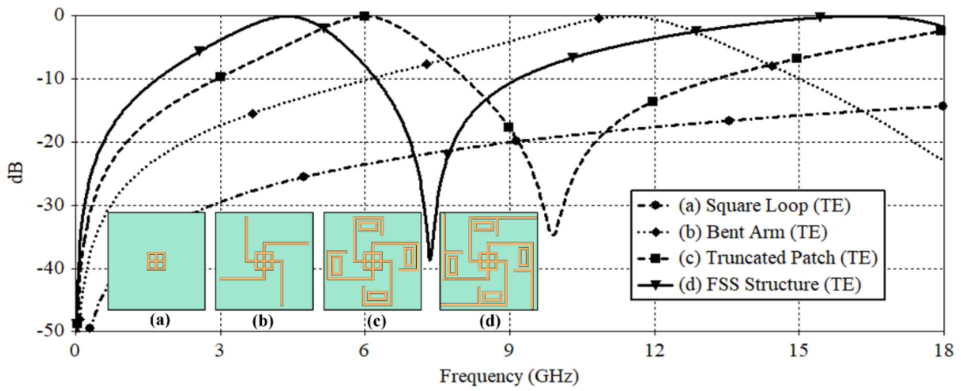

Figure 2. *Simulated S_{11} characteristics corresponding to the sequential design stages.*

The proposed FSS unit cell is optimized to exhibit a high-selectivity band-pass characteristic within the 6.2–9.1 GHz frequency range. Upon analyzing the return loss (S_{11}) data presented in Fig. 3, it is observed that the structure achieves a resonance depth below -35 dB at its center frequency. This performance, which stays significantly below the conventional -10 dB threshold, indicates reduced reflection within the operational band and supports efficient transmission through the structure. Furthermore, the FSS exhibits a robust suppression characteristic outside the passband, demonstrating distinct band-stop behavior in the 4–4.7 GHz and 15–17.3 GHz ranges, thereby reinforcing its overall frequency selectivity. Moreover, the nearly identical overlap between the TE and TM modes across both the band-pass and band-stop regions further supports the polarization-insensitive response expected from the symmetric unit-cell geometry.

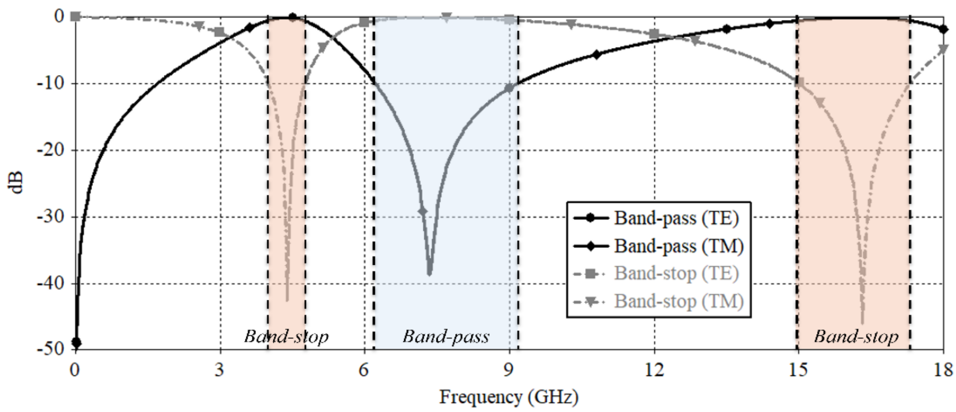

Figure 3. *Simulated reflection (S_{11}) and transmission (S_{21}) coefficients of the proposed FSS under normal incidence for TE and TM modes.*

The performance characteristics of the proposed band-pass FSS were further analyzed using the absolute bandwidth, Fractional Bandwidth (FBW), and Quality Factor (Q-factor) at normal incidence. Based on the -10 dB impedance bandwidth, the lower and upper cut-off frequencies were determined as 6.229 GHz and 9.169 GHz, respectively, yielding a center frequency of 7.344 GHz. The structure provides a broad operating bandwidth of 2.94 GHz, which corresponds to a significant FBW of 40.03% and a Q-factor of 2.50.

To quantitatively substantiate the high selectivity of the proposed FSS, the roll-off rates at both edges of the pass-band were calculated. On the lower frequency side, the design demonstrates a maximum roll-off rate of 40.15 dB/GHz, as the response transitions from -3.07 dB at 5.33 GHz to a deep suppression level of -40.93 dB at 4.39 GHz. On the higher frequency side, the structure achieves a roll-off rate of 11.02 dB/GHz, shifting from -3.02 dB at 12.43 GHz to a peak attenuation of -45.96 dB at 16.32 GHz. These values indicate a highly selective frequency response and support out-of-band interference suppression for CubeSat-oriented communication systems.

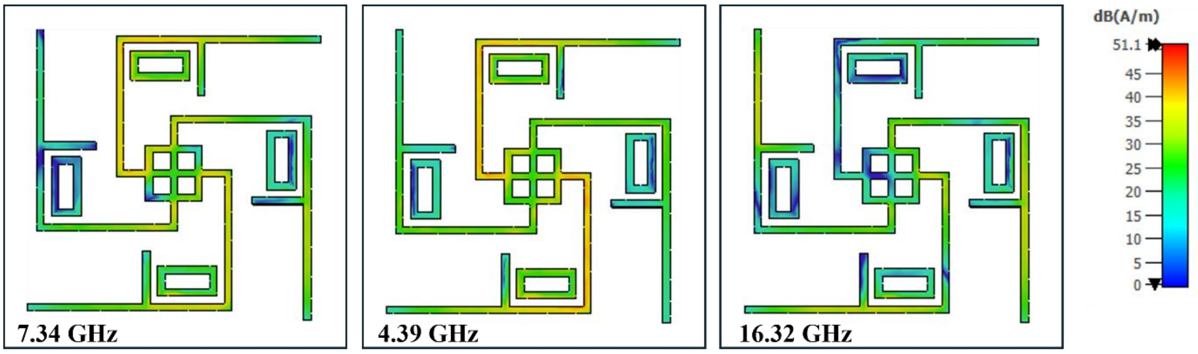

Figure 4. *Surface current distributions of the proposed FSS unit cell at: (a) 7.34 GHz, (b) 4.39 GHz, and (c) 16.32 GHz.*

To physically validate the operating principle and band selectivity of the proposed FSS, the surface current distributions are investigated at critical frequencies within the transmission and rejection bands (Fig. 4). At the resonance frequency of 7.34 GHz, as shown in Fig. 4 (a), the surface current is observed to bypass the outer frame and distribute homogeneously across the square loop and the truncated patch geometries. Although the current paths may visually resemble those at the stop-band, at 7.34 GHz, the induced currents on the adjacent metallic traces exhibit a phase relationship that generates a parallel LC resonance. This behavior confirms that the structure achieves impedance matching with free space and becomes "electrically transparent" at this frequency, allowing the EM energy to transmit with minimal insertion loss. In contrast, at the lower stop-band of 4.39 GHz (Fig. 4(b)), the current density is sharply confined to the bent arm structures and the outermost frame. At this specific frequency, the phase and intense concentration of the currents act entirely as a dominant series inductance, causing a severe impedance mismatch. These elements act as a high series inductance, creating a highly reflective shield that prevents the energy from penetrating the inner resonator parts. Similarly, at the high-frequency rejection region of 16.32 GHz (Fig. 4(c)), the current exhibits a fragmented distribution within the overall structure, indicating the excitation of higher-order modes that facilitate a wide-band suppression characteristic. Overall, the current confinement within the bent arms during rejection and its distribution over the square loop and truncated patches during resonance support the proposed filtering mechanism, explaining the high selectivity of 40.15 dB/GHz achieved by the proposed design.

The Shielding Effectiveness (SE) of the proposed FSS is a vital metric to quantify its ability to suppress EMI. In this study, the SE is directly derived from S_{21} magnitude as SE (dB) = -S_{21} (dB) at normal incidence (θ = 0°). According to the simulation results, the structure exhibits high shielding effectiveness in both rejection bands. Specifically, at the lower stop-band center frequency of 4.39 GHz, the SE reaches 40.94 dB, providing more than 99.99% power suppression against interfering signals. Furthermore, the SE value reaches its peak at 45.97 dB within the upper rejection band at 16.32 GHz. These SE levels indicate that the proposed FSS can contribute to suppressing out-of-band interference in CubeSat-oriented RF front-end or shielding applications.

3.2. Parametric Analysis

The primary objective of the design is to facilitate the transmission of signals within the targeted 7–9 GHz X-band, while providing robust EM suppression specifically within the dual band-stop regions (4–4.7 GHz and 15–17.3 GHz). To achieve this, extensive parametric studies were performed on the critical geometric dimensions (L_1, L_2 and L_6) that significantly influence the resonance frequency of the structure. The detailed results of these analyses and their impact on the frequency response are illustrated in Fig. 5.

The physical mechanism governing these frequency shifts can be explained using the equivalent circuit model of the FSS, where the resonance frequency is determined by $f_r = 1/2\pi\sqrt{LC}$. In this model, the metallic traces primarily contribute to the equivalent inductance (L), whereas the gaps between the adjacent elements generate the equivalent capacitance (C). Consequently, enlarging the physical dimensions of the metallic strips increases the effective electrical length, which directly enhances the equivalent inductance and forces the resonance frequency to shift downward.

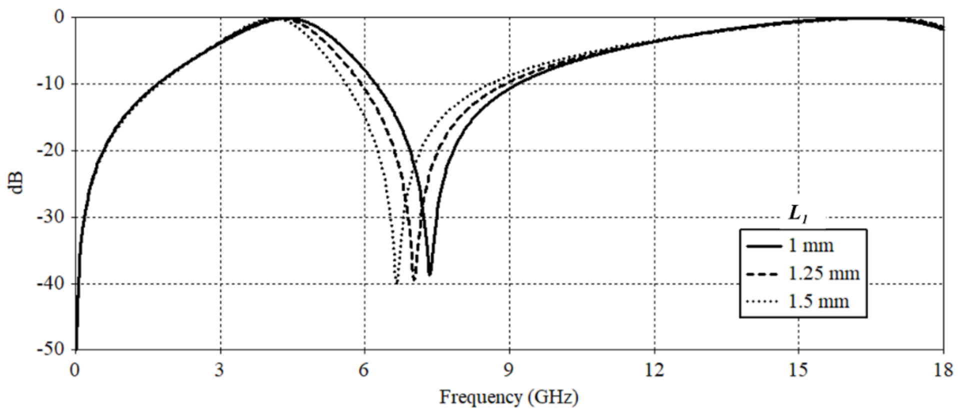

(a)

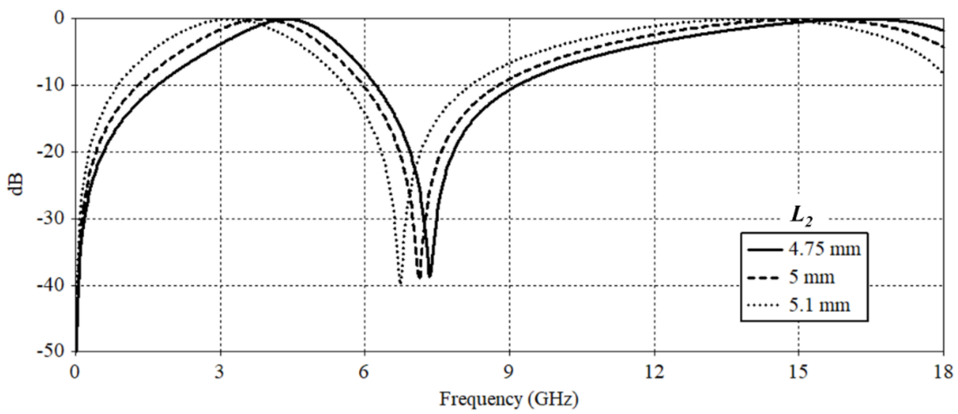

(b)

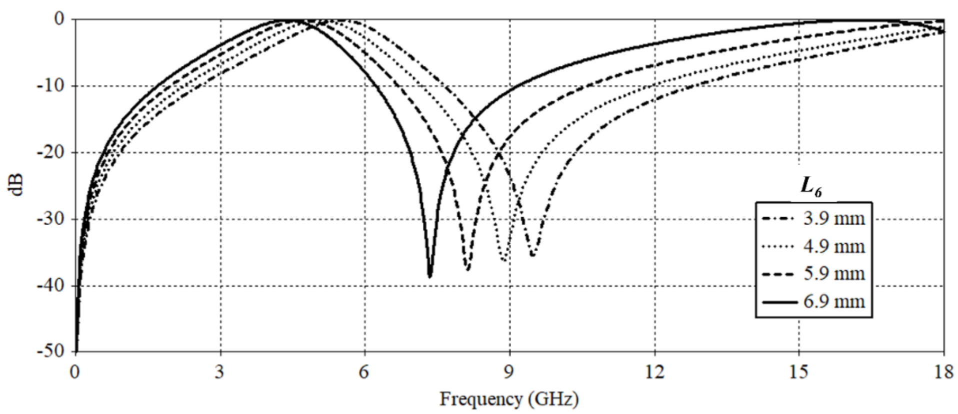

(c)

Figure 5. *Effects of the critical geometric parameters on S_{11} of the proposed FSS structure: (a) L_1, (b) L_2, and (c) L_6.*

The simulation results regarding the L_1 parameter, which represents the length of the short edge connecting the bent arm to the square loop, are presented in Fig. 5(a). As the value of L_1 increases, the extended surface current path proportionally increases the equivalent series inductance, causing the resonance frequency to shift toward lower frequencies (leftward). Similarly, as shown in Fig. 5(b), an increase in the L_2 parameter, representing the long edge of the bent arm, elongates the effective electrical length and yields a pronounced downward frequency shift. Consistent with these findings, extending the L_6 parameter introduces additional inductive loading to the unit cell, which further shifts the center frequency to the left, as depicted in Fig. 5(c). Through this parametric optimization, the final dimensions were tuned to align the passband and stopband characteristics with the targeted spectrum.

3.3. Cross-Polarization Analysis

The cross-polarization performance of the proposed FSS is analyzed to assess polarization isolation for both band-pass and band-stop operations under varying incidence angles. Fig. 6(a) illustrates the cross-polarization isolation for the band-pass region (S_{11}^{cross}). These specific leakage levels should be evaluated in conjunction with the primary co-polarized transmission characteristics previously detailed in Fig. 3 and Fig. 7. At normal incidence (θ = 0°), the isolation levels are remarkably high, staying below -60 dB. More importantly, under an extreme oblique incidence of θ = 60°, the cross-polarization levels within the operational pass-band remain consistently below -20 dB (specifically marked at -27.57 dB and -20.67 dB for the targeted frequencies). This result indicates that even at highly tilted angles, the isolation between orthogonal states is maintained at a robust level, which is a critical requirement for secure CubeSat communication links.

Furthermore, Fig. 6(b) presents the cross-polarization characteristics for the band-stop regions (S_{21}^{cross}). At the lower rejection frequency of 4.39 GHz, the structure maintains an excellent isolation of -43.97 dB even at θ = 60°. Although the isolation levels naturally tend to increase at higher frequencies and larger incidence angles due to the projected structural asymmetry, the overall cross-polarization suppression remains within the targeted isolation range over the main operating band. The stability of these results across a wide angular range from 0° to 60° demonstrates that the proposed unit cell's rotational symmetry effectively minimizes mode conversion, supporting a stable filtering response under the simulated oblique-incidence conditions. The complementary nature of the responses in Figures 6(a) and 6(b) provides a comprehensive view of the circuit's operation, effectively demonstrating the transition between the band-pass and band-stop regions.

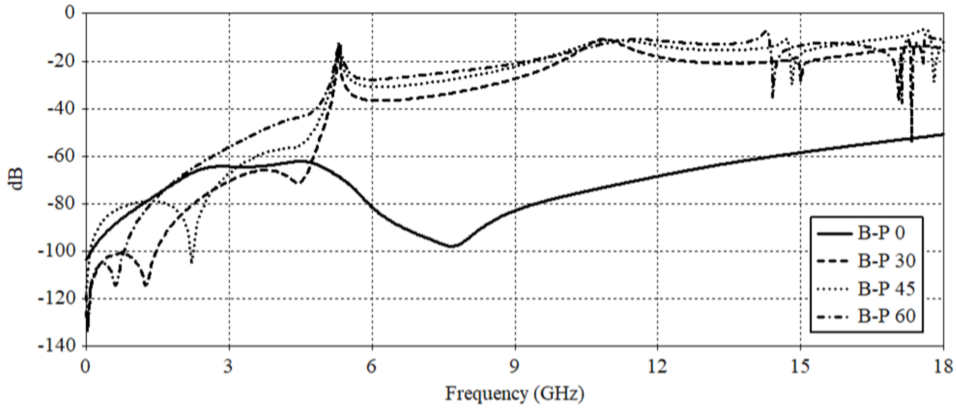

(a)

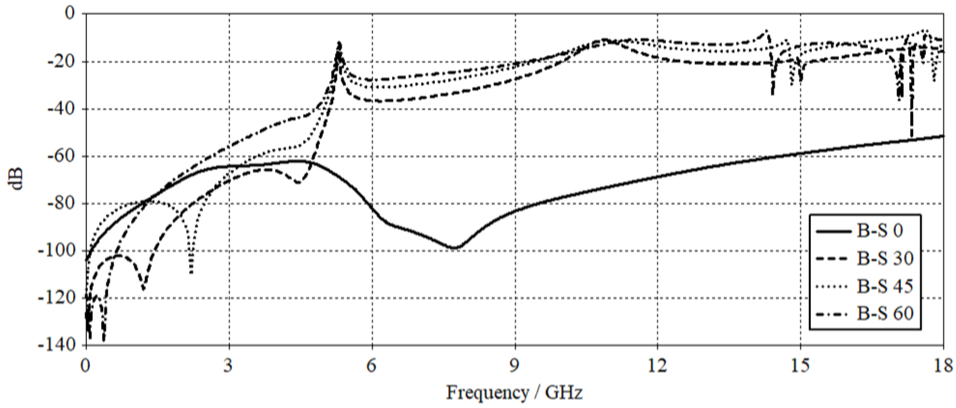

(b)

Figure 6. *Simulated cross-polarization coefficients under various incidence angles (θ): (a) reflection coefficient (S_{11}^{cross}) and (b) transmission coefficient (S_{21}^{cross}).*

3.4. Angular Stability Analysis

The transmission characteristics of the proposed FSS structure under varying angles of incidence (θ) from 0° to 60° for both TE and TM polarization modes are depicted in Fig. 7. Specifically, at normal incidence, the structure provides a wide pass-band covering the 6.2–9.1 GHz range. However, at extreme oblique angles such as 60°, a noticeable bandwidth narrowing occurs, particularly for the TE polarization, where the upper cut-off frequency shifts downward, reducing the pass-band to approximately 6.3–8.0 GHz. This bandwidth degradation is an expected phenomenon in single-layer periodic structures, primarily attributed to the variation of the effective free-space wave impedance ($Z_{TE} = Z_0 / \cos\theta$) at highly oblique incidences, which deteriorates the optimal impedance matching condition. Additionally, the change in the projected electrical length of the unit cell at steep angles affects the mutual coupling. Nevertheless, despite this inherent bandwidth narrowing at 60°, the core resonance around the center frequency (7.34 GHz) remains highly stable with minimal insertion loss, indicating that the design maintains its core filtering profile for the targeted CubeSat sub-bands.

Furthermore, a similar angular dependency is observed in the dual band-stop regions. The first rejection band (4–4.7 GHz) is virtually insensitive to the incidence angle, with transmission nulls consistently maintaining deep EM suppression levels below -40 dB regardless of the wave's arrival angle. Conversely, while the second stop-band (15–17.3 GHz) provides robust shielding at normal and moderate angles, a noticeable frequency shift and a reduction in resonance depth are observed at extreme oblique incidences, particularly for the TM mode at 60˚. This deviation at higher frequencies is primarily attributed to the potential excitation of grating lobes as the operating wavelength becomes comparable to the unit cell dimensions at extreme oblique incidences. Overall, the proposed design maintains a stable core filtering response across the targeted lower-frequency bands under simulated oblique-incidence conditions, while some degradation appears at higher frequencies and larger incidence angles.

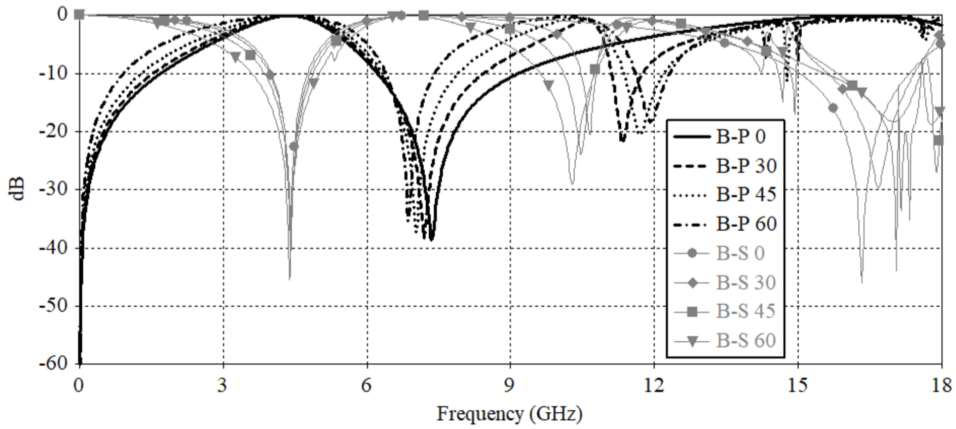

(a)

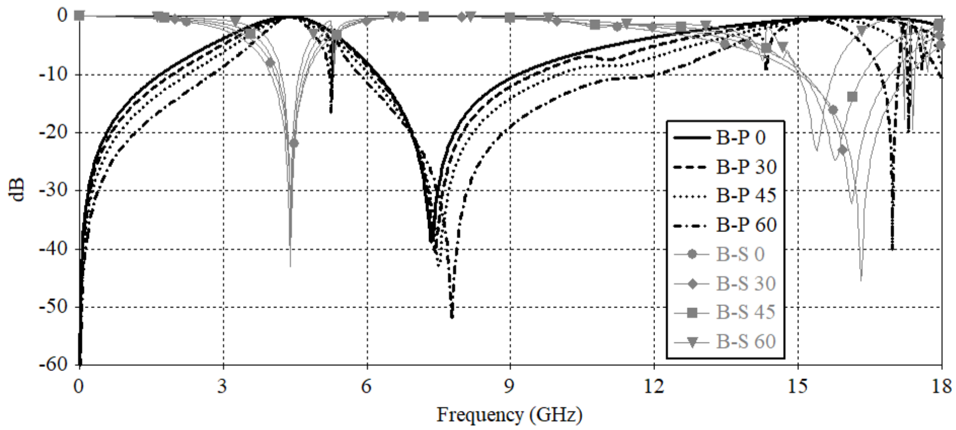

(b)

Figure 7. *Simulated S_{21} of the proposed FSS under various oblique incidence θ angles from 0˚ to 60˚: (a) TE mode, and (b) TM mode. (B-P Band-pass, B-S Band-stop).*

4. FABRICATION AND MEASUREMENT RESULTS

This section describes the fabrication process and free-space measurement validation of the proposed FSS design. As a proof of concept, the structure is intended for integration onto a 1U CubeSat platform to provide EM shielding and highly selective filtering, as illustrated in the 3D simulation model (Fig. 8a). Based on this application scenario, a physical prototype of the FSS array was fabricated utilizing high-precision printed circuit board (PCB) manufacturing techniques. A comparison between the simulation model and the fabricated prototype (Fig. 8b) shows that the main geometrical features of the design were successfully realized. Furthermore, the close-up view of the manufactured unit cell (Fig. 8c) demonstrates the precise realization of the optimized complex geometry. To experimentally validate the filtering performance, the manufactured prototype was characterized via the free-space measurement method within a controlled clean room laboratory environment. During the measurements, the FSS prototype was carefully positioned on a low-permittivity foam stand between the transmitting and receiving antennas to minimize structural interference. The experimental setup employed two wideband Schwarzbeck BBHA 9120 D horn antennas (operating between 1–18 GHz) connected to a Keysight N5245A PNA-X Microwave Network Analyzer, which was precisely calibrated using the standard Short-Open-Load-Through (SOLT) technique. Furthermore, to accurately characterize S_{11} and establish the precise 0 dB reference level shown in the measurements, a free-space normalization procedure was conducted. A solid metallic plate (perfect electric conductor - PEC) with physical dimensions identical to the FSS array was placed at the exact measurement plane. The reflection response of this metallic plate was measured and utilized as the 0 dB baseline to compensate for the free-space path loss and the phase center variations of the horn antennas.

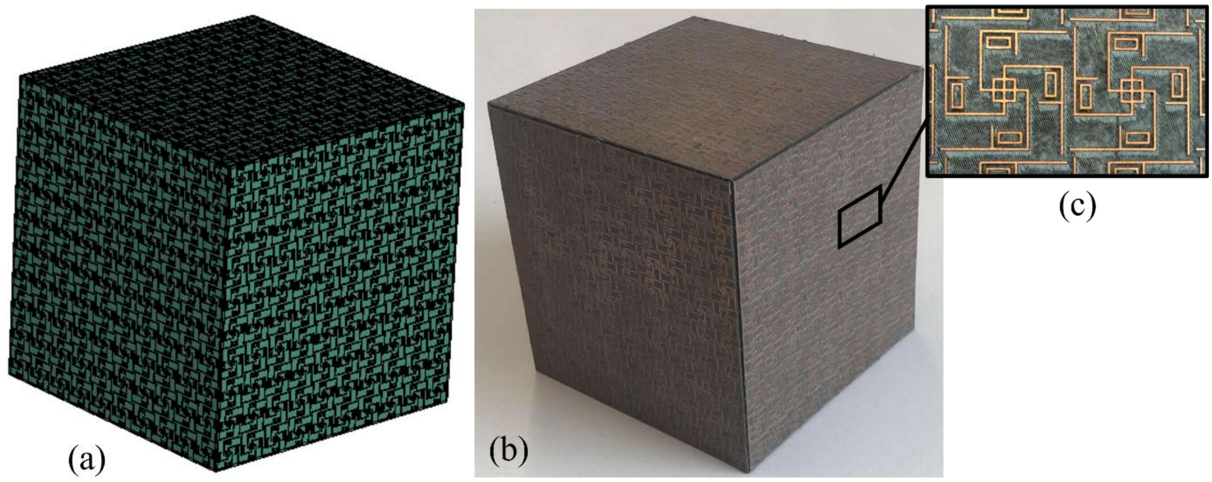

Figure 8. *Integration and fabrication of the proposed FSS for space applications: (a) 3D simulation model on a 1U CubeSat platform, (b) the fabricated FSS prototype, and (c) a close-up view of the manufactured unit cell.*

The experimental setup used for the free-space measurements is depicted in Fig. 9a. Experimental angular-stability measurements under oblique incidence were not performed in the present study because the available clean-room facility did not include a dedicated bi-static angular free-space measurement setup. Therefore, the angular-stability assessment is based on the full-wave TE/TM oblique-incidence simulations in Fig. 7, whereas the experimental validation is limited to the normal-incidence filtering response. Following this, the comparison between the simulated and measured responses for TE mode under normal incidence (θ = 0°) is evaluated. Fig. 9b illustrates the measured and simulated pass-band responses. The experimental results show that the fabricated prototype exhibits a band-pass characteristic that generally follows the simulated 6.2–9.1 GHz response. However, a slight bandwidth narrowing and a marginal frequency shift, accompanied by a minor insertion loss, are observed in the measured pass-band. Similarly, Fig. 9c presents the measured and simulated rejection responses for the dual band-stop regions. The prototype demonstrates robust EM suppression specifically at the 4–4.7 GHz and 15–17.3 GHz bands, with measured rejection levels reaching deep resonance dips that highly correlate with the full-wave simulation predictions.

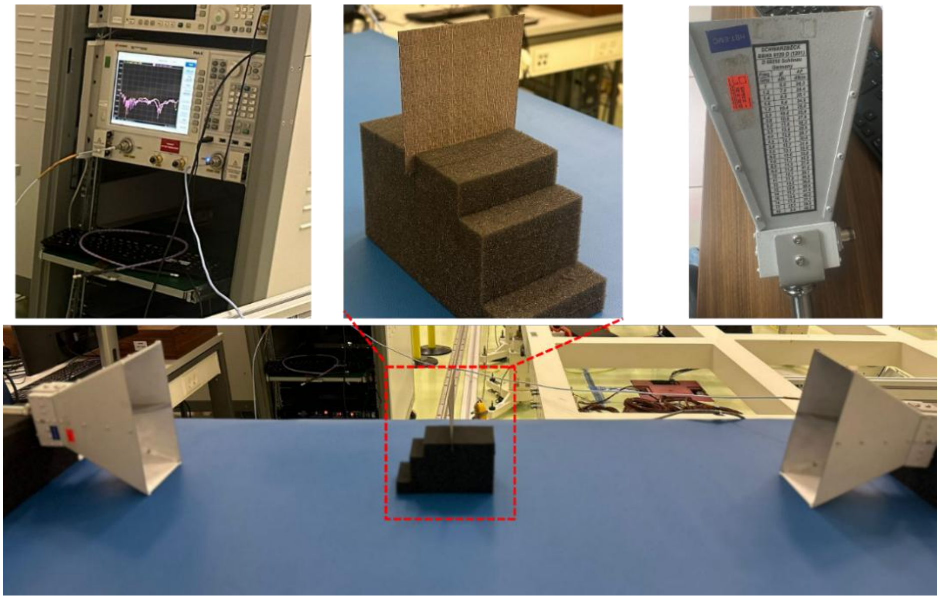

(a)

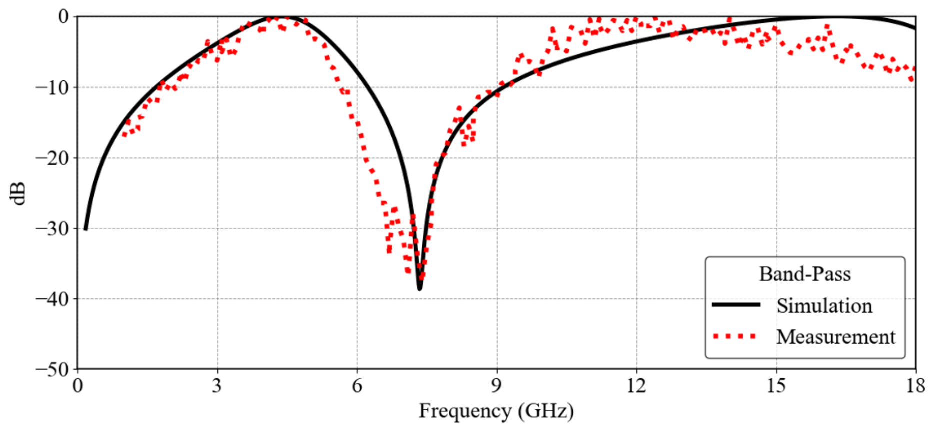

(b)

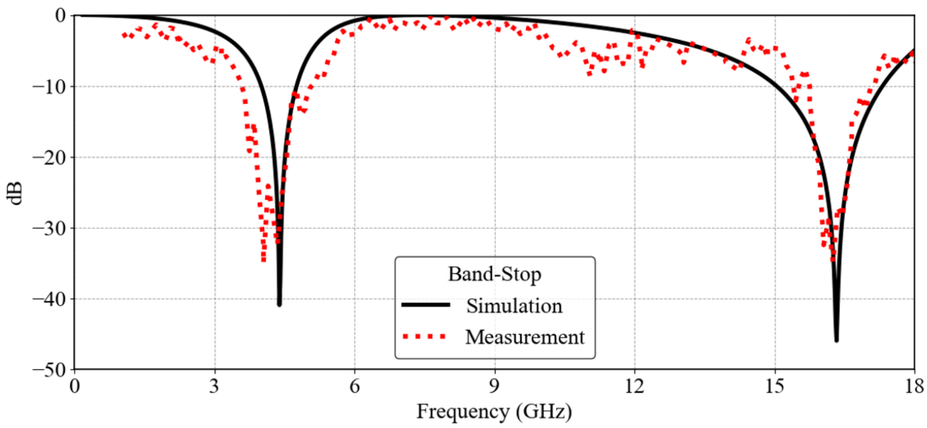

(c)

Figure 9. *Experimental validation of the proposed FSS: (a) free-space measurement setup in the clean-room laboratory, (b) comparison of simulated and measured pass-band responses (TE mode), and (c) comparison of simulated and measured dual band-stop responses (TE mode).*

Although there is an excellent overall agreement between the measured and simulated data, the minor discrepancies, such as the slight bandwidth fluctuations, frequency shifts, and reduced resonance depths, are expected in practical realizations. These deviations can be primarily attributed to fabrication tolerances during the PCB manufacturing process (e.g., over-etching or under-etching), which slightly alter the effective electrical length of the resonant elements. Additionally, the finite size of the fabricated FSS array introduces edge diffraction and scattering effects, which inherently differ from the infinite periodic boundary conditions assumed in the simulations. Finally, minor alignment imperfections and unavoidable spurious reflections within the clean-room measurement set-up contribute to these slight variations. Nevertheless, the agreement between the simulated and measured normal-incidence responses supports the feasibility of the proposed FSS as a compact EM filtering and shielding structure for CubeSat-oriented applications.

To quantitatively evaluate the performance characteristics and structural features of the proposed design, its critical electromagnetic metrics are benchmarked against recently reported FSS structures from the literature, as systematically summarized in Table 2.

Table 2. *Comparison of the proposed FSS with related works in the literature.*

Ref. (Year)	Unit Cell Size & Thickness (λ_0)	Center Freq. (GHz)	Filter Type	Layer Structure	FBW (%)	Selectivity / Roll-off	Peak SE (dB)	Pol. Indep.	Ang. Stab.
[17] (2025)	0.0096 ×0.0096 / 0.0009	268	Band-pass	2.5D / 4 Vias	87.0	Low Q-Factor (Gradual)	Harmonic Suppression	Yes	60°
[18] (2022)	0.1 ×0.1 / 0.32	~5.0	Band-pass	3D PCB	38.3	3 Transmission Poles	>10 dB (7-14 GHz)	Yes	60°
[19] (2018)	0.26 ×0.26 / 0.018	7.15, 13.02 (Pass)8.22 (Stop)	Dual Pass / Single Stop	3 Metallic Layers	25.0 / 65.6	2nd-Order Filtering	>26.4 dB / >29.7 dB	Yes	75°
[20] (2025)	0.216 ×0.216 / 0.0029	2.95, 10.05 (Pass)5.68 (Stop)	Dual Pass / Single Stop	Ultrathin Single Layer	34.3 / 23.6	Limited (No TZs)	45.7 dB	Yes	60°
[21] (2026)	0.12 ×0.12 / 0.068	7.2 / 12.6	Dual Band-pass (PSS)	5 Layers (Prepreg)	19.0 / 31.0	3rd-Order (FSFM: 0.65)	Sub-resonance	No	45°
[22] (2020)	0.2 ×0.2 / 0.0325	6.0	Band-pass	Double Layer	5.1	Quasi-Elliptic (2 TZs)	>20 dB	Yes	40°
[23] (2025)	0.17 ×0.17 / 0.18	~27.75 (K-Ka)	Ultra-Wideband Pass	Multilayer	68.1	LC Resonance	Extended Attenuation	Yes	±40°
This Work	0.206 ×0.206 /0.016	7.34	Band-pass / Dual Band-stop	Single Layer	40.03	Max. 40.15 dB/GHz	>45 dB	Yes (< -20 dB)	60°

The comparison in Table 2 highlights the main performance features of the proposed FSS relative to recent related works. While several advanced filters in the literature achieve high selectivity or dual-polarized functionality, some reported designs employ multilayer topologies [19], [21], [23], internal vertical via arrays [17], or multi-layered PCB configurations [18], [22], which significantly increase total profile thickness, fabrication costs, and spatial alignment errors. By comparison, the proposed design achieves a maximum roll-off rate of 40.15 dB/GHz and a deep out-of-band shielding effectiveness exceeding 45 dB by utilizing a strictly single-layer metallization profile with an ultrathin configuration (0.016 λ_0). Furthermore, unlike designs that exhibit significant performance degradation or severe cross-polarization leakage under oblique angles, the proposed structure maintains its main filtering response and cross-polarization isolation levels below -20 dB up to 60° incidence in simulation. Consequently, the proposed FSS offers a favorable balance between structural simplicity, frequency selectivity, and angular stability for low-profile CubeSat-oriented RF applications.

5. CONCLUSION

In this study, a highly selective, polarization-independent band-pass FSS is proposed for CubeSat-oriented communication applications, and its normal-incidence filtering response is experimentally validated. The primary novelty of the proposed design lies in its four-fold symmetric architecture, which supports polarization-insensitive behavior and stable core filtering performance up to 60° oblique incidence in full-wave simulations. Experimental and simulation results at normal incidence confirm that the FSS exhibits a wide pass-band from 6.2 to 9.1 GHz, achieving an FBW of 40.03%, covering the targeted 7–9 GHz communication band. Furthermore, the structure demonstrates high frequency selectivity with a maximum roll-off rate of 40.15 dB/GHz while simultaneously providing deep dual band-stop responses at 4–4.7 GHz and 15–17.3 GHz. The peak SE exceeding 45 dB indicates more than 99.99% power suppression at the rejection-band resonance, suggesting its potential to reduce out-of-band interference in CubeSat-oriented RF front-end applications. For future work, the proposed FSS will be integrated and tested with the internal electronic systems of a functional 1U CubeSat platform to evaluate its real-world EM shielding performance. In addition, future studies will focus on co-designing and integrating the FSS with a dedicated satellite antenna operating in the pass-band region to investigate its influence on antenna radiation characteristics, such as gain, directivity, and impedance matching.

✵ ✵ ✵

Peer-review: External, Independent.

Acknowledgements:
The authors have no acknowledgements to declare.

Declarations:

1. Statement of Originality:
The authors declare that this manuscript is original, has not been published previously, and is not currently under consideration for publication elsewhere.

2. Author Contributions:
Concept: MG,MK,HJ,GOA; ***Conceptualization:*** MG,MK,HJ,GOA; ***Literature Search:*** MG,MK,HJ,GOA; ***Data Collection:*** MG,MK,HJ,GOA; ***Data Processing:*** MG,MK,HJ,GOA; ***Analysis:*** MG,MK,HJ,GOA; ***Writing – original draft:*** MG,MK,HJ,GOA; ***Writing – review & editing:*** MG,MK,HJ,GOA.

3. Ethics approval:
Not applicable. This study does not involve human participants, human data, or animals. All evaluations were conducted through computer simulations, prototype fabrication, and laboratory measurements using technical equipment.

4. Funding/Support:
This research received no specific grant, funding, or financial support from any public, commercial, or not-for-profit funding agency.

5. Competing Interests:
The authors declare that they have no competing financial interests or personal relationships that could have appeared to influence the work reported in this paper.

6. GenAI Usage Statement:
GenAI tools were not used to generate scientific results, simulation data, experimental measurements, figures, or technical interpretations in this study. GenAI-assisted language editing was used only to improve grammatical accuracy, readability, and editorial clarity. All scientific content, technical claims, numerical results, and conclusions were checked and approved by the authors.

7. Sustainable Development Goals:

REFERENCES

[1] M. Karahan, E. Aksoy, ve Y. Yavuz, “A frequency selective surface design to reduce the interference effect on satellite communication”, içinde *2017 8th International Conference on Recent Advances in Space Technologies (RAST)*, Istanbul, Turkey: IEEE, Haz. 2017, ss. 221-223. doi: 10.1109/RAST.2017.8003013.

[2] B. Karibayev, T. Namazbayev, G. Ikhsan, B. Kozhakhmetova, ve S. Arzykulov, “Frequency-Based Classification of Practical CubeSat Antennas: A Review”, *IEEE Access*, c. 13, ss. 178112-178147, 2025, doi: 10.1109/ACCESS.2025.3620808.

[3] R. Anwar, L. Mao, ve H. Ning, “Frequency Selective Surfaces: A Review”, *Appl. Sci.*, c. 8, sy. 9, s. 1689, Eyl. 2018, doi: 10.3390/app8091689.

[4] M. Karahan ve E. Aksoy, “Design and analysis of angular stable antipodal F-type frequency selective surface with multi-band characteristics”, *Int. J. RF Microw. Comput.-Aided Eng.*, c. 30, sy. 12, Ara. 2020, doi: 10.1002/mmce.22466.

[5] S. M. Q. A. Shah, F. Ahmed, ve N. Shoaib, “A Miniaturized FSS Based Band-Stop Filter for EMI Shielding Applications”, içinde *2020 International Conference on UK-China Emerging Technologies (UCET)*, Glasgow, United Kingdom: IEEE, Ağu. 2020, ss. 1-3. doi: 10.1109/UCET51115.2020.9205483.

[6] W. Li ve Y. Li, “A High Selectivity, Miniaturized, Low Profile Dual-Band Bandpass FSS with a Controllable Transmission Zero”, *Int. J. Antennas Propag.*, c. 2017, ss. 1-9, 2017, doi: 10.1155/2017/7983567.

[7] J. Ghosh, R. Dutta, A. Sarkhel, ve Q. H. Abbasi, “Design of miniaturize flexible wideband frequency selective surface for electromagnetic shielding application”, *Waves Random Complex Media*, c. 35, sy. 6, ss. 11249-11269, Kas. 2025, doi: 10.1080/17455030.2022.2121442.

[8] W. Afzal, M. Z. Baig, A. Ebrahimi, Md. R. Robel, M. T. A. Rana, ve W. Rowe, “Frequency Selective Surfaces: Design, Analysis, and Applications”, *Telecom*, c. 5, sy. 4, ss. 1102-1128, Kas. 2024, doi: 10.3390/telecom5040056.

[9] K. Sarabandi ve N. Behdad, “A Frequency Selective Surface With Miniaturized Elements”, *IEEE Trans. Antennas Propag.*, c. 55, sy. 5, ss. 1239-1245, May. 2007, doi: 10.1109/TAP.2007.895567.

[10] P.-C. Zhao, Z.-Y. Zong, W. Wu, ve D.-G. Fang, “A Convoluted Structure for Miniaturized Frequency Selective Surface and Its Equivalent Circuit for Optimization Design”, *IEEE Trans. Antennas Propag.*, c. 64, sy. 7, ss. 2963-2970, Tem. 2016, doi: 10.1109/TAP.2016.2565694.

[11] C. Sun *vd.*, “A dual-band dual-polarization metasurface filter with high-selectivity passband and wide-angle stability properties”, *J. Phys. Appl. Phys.*, c. 58, sy. 41, s. 415003, Eki. 2025, doi: 10.1088/1361-6463/ae0a65.

[12] Q. Chen, S. Yang, J. Bai, ve Y. Fu, "Design of Absorptive/Transmissive Frequency-Selective Surface Based on Parallel Resonance", *IEEE Trans. Antennas Propag.*, c. 65, sy. 9, ss. 4897-4902, Eyl. 2017, doi: 10.1109/TAP.2017.2722875.

[13] S. Xi, K.-D. Xu, S. Yang, X. Ren, ve W. Wu, "X-band frequency selective surface with low loss and angular stability", *AEU - Int. J. Electron. Commun.*, c. 173, s. 154990, Oca. 2024, doi: 10.1016/j.aeue.2023.154990.

[14] A. Gouda ve S. Ghosh, "An analytical study of curved frequency selective surfaces for shielding applications", *Microw. Opt. Technol. Lett.*, c. 65, sy. 12, ss. 3139-3146, Ara. 2023, doi: 10.1002/mop.33851.

[15] M. Karahan ve E. Aksoy, "Design of a PIN Diode-Based Reconfigurable Frequency Selective Surface", içinde *2022 Workshop on Microwave Theory and Techniques in Wireless Communications (MTTW)*, Riga, Latvia: IEEE, Eki. 2022, ss. 95-99. doi: 10.1109/MTTW56973.2022.9942460.

[16] M. Karahan, Y. Yavuz, S. H. Ates, ve E. Aksoy, "A Dual-Band Frequency Selective Surface Structure with Stable Performance for Oblique Incidence".

[17] J. A. Vásquez-Peralvo *vd.*, "2.5D Inductive Intertwined Frequency Selective Surface for Band-Pass and High Miniaturization Applications", *IEEE Access*, c. 13, ss. 22156-22165, 2025, doi: 10.1109/ACCESS.2025.3535565.

[18] S. Feng, Y. Han, X. Xiu, W. Che, ve Q. Xue, "Design of a Three-dimensional Bandpass Frequency Selective Surface Based on Coupled-slotlines", içinde *2022 IEEE MTT-S International Microwave Workshop Series on Advanced Materials and Processes for RF and THz Applications (IMWS-AMP)*, Guangzhou, China: IEEE, Kas. 2022, ss. 1-3. doi: 10.1109/IMWS-AMP54652.2022.10107306.

[19] A. N. Biswas, S. Ballav, S. K. Parui, ve A. Chatterjee, "A Polarization Insensitive Frequency Selective Surface with Bandpass and Bandstop Response", içinde *2018 IEEE Indian Conference on Antennas and Propogation (InCAP)*, Hyderabad, India: IEEE, Ara. 2018, ss. 1-4. doi: 10.1109/INCAP.2018.8770800.

[20] K. P. Kaur, M. L. S. N. S. Lakshmi, S. Kaur, ve S. Ralhan, "Numerical and Equivalent-Circuit Analysis of Ultrathin FSS With Wide-Stopband Response for EM Shielding Applications", içinde *2025 Fifth International Conference on Advances in Electrical, Computing, Communication and Sustainable Technologies (ICAECT)*, Bhilai, India: IEEE, Oca. 2025, ss. 1-7. doi: 10.1109/ICAECT63952.2025.10958900.

[21] F. J. Hidalgo, R. R. Boix, M. Camacho, ve J. Córcoles, "Optimized Design of a Dual-Band Polarization Selective Surface with Third-Order Band-Pass Responses Using In-House Method of Moments", *IEEE Antennas Wirel. Propag. Lett.*, ss. 1-5, 2026, doi: 10.1109/LAWP.2026.3690976.

[22] R.-X. Liao *vd.*, "Quasi-Elliptic Bandpass Frequency Selective Surface Based on Coupled Stubs-Loaded Ring Resonators", *IEEE Access*, c. 8, ss. 113675-113682, 2020, doi: 10.1109/ACCESS.2020.3003319.

[23] S.-L. Yang, F.-S. Zhang, L.-W. Song, ve F. Zhang, "Frequency-Selective Surface With Dual Polarization and Ultrawide Passband", *IEEE Trans. Antennas Propag.*, c. 73, sy. 4, ss. 2510-2520, Nis. 2025, doi: 10.1109/TAP.2025.3539960.

✵ ✵ ✵